TECHNICAL REVIEW

No.22 / September 2024

Technical Review

MAPNA TURBINE ENGINEERING & MANUFACTURING CO. (TUGA)

TUGA

MAPNA GROUP

Willpower to Empower Generations

TECHNICAL REVIEW

Editorial & Production

Cover Page:
MGT-70 Assembly Platform

Editorial

Dear Colleagues, Partners and Professionals,

Here at MAPNA Turbine (TUGA), we constantly endeavor to extend our influence in the market and create value for our customers by further developing our products and methods, as well as portfolio of services. It is in this context and with great pleasure that a brief account of a few recent technological achievements is presented to you, our valued readers, in this edition of TUGA Technical Review.

As the main manufacturer of heavy-duty gas turbines in Iran, TUGA is committed to delivering comprehensive support for its products. The first article reviews the overall and detailed engineering, supply and manufacturing, commissioning, and testing of the latest upgrade for MGT-70 fleet (MAP2C), aimed at increasing the turbine's power output capacity and enhancing the lifecycle performance of critical hot-section components.

Considering technological and metallurgical limitations in the production process of MGT-30 fleet nozzle vanes, repair and refurbishment of these vanes instead of replacing them can bring about high added value. In the second article, failure mechanisms and steps of the refurbishment process are outlined for the first two stages of stationary hot blades of this turbine.

The third article investigates the DIA (Drop Image Analysis) technique as a prominent optical approach to measure the diameter of spray droplets produced by the liquid fuel injectors. Adopting this method in combustion laboratories represents a simple, cost-effective, and accurate approach in advancing the knowledge of designing gas turbine injection systems.

Burners and turbine blades are among the key components in a gas turbine through which flow rates affect the overall performance of the machine. The fourth article focuses on the new airflow test stand manufactured in TUGA to test these components, which can improve the manufacturing process by reducing cost and time, leading to optimal performance.

In the last article, the need to measure some instantaneous time parameters regarding the diesel injection is fulfilled by implementing an innovative, cost-effective, and experimental method using high-speed shadowgraphy and a simple optical trick. The data acquired from this experimental study will be used in combustion investigations to assess engine performance and component lifetime studies.

Please join us in relishing a detailed account of these subjects in this issue of the Technical Review.

Respectfully,

Roohollah Jabery,

Vice President for Engineering and R&D

MAPNA Turbine Company (TUGA)

September 2024

Contents

1

Introducing MAP2C Upgrade for MGT-70 Fleet

Hashemi, Omidreza
Jafari, Niloofar
KhaniGouabad, Abbas

MAPNA Turbine Engineering & Manufacturing Co. (TUGA)

Introduction

TUGA is recognized as the main manufacturer and supplier of heavy-duty gas turbines in Iran, notably distinguished for its renowned MGT-70 fleet gas turbines, with over 190 operational units deployed nationwide. As a matter of corporate responsibility, TUGA is committed to delivering comprehensive support for its MGT-70 fleet, encompassing continuous improvement and development initiatives. This dedication has yielded three successive upgrades over the past decade, reflecting the company's ongoing commitment to enhancing the performance and reliability of its products. Continuing this trajectory of advancement, TUGA initiated the development of the fourth-generation MGT-70(4) upgrade in 2019. This latest upgrade aimed at increasing the turbine's power output capacity and enhancing the lifecycle performance of critical hot-section components.

Major Project Milestones

The combination of a complex economic environment, high demand for power, lack of incentive for companies to build new power plants, and the growing adoption of sustainable power generation methods has created a challenging situation for power generation companies. Considering all these key parameters, TUGA has prioritized enhancing the performance characteristics and reducing maintenance costs of its fleet, while minimizing additional costs and modifications compared to its previous upgraded versions. A comprehensive feasibility study was conducted to investigate various upgrade scenarios, to identify the most suitable program that aligned with customer needs and priorities.

The MGT-70(4) has been developed in the following main phases:

- Feasibility study of upgrading scenarios
- Detail design and analysis of components
- Review of manufacturing criteria
- Development of manufacturing process of upgraded elements
- Implementation of upgraded version
- Commissioning and performance test

Improvements to the new upgraded version could be either in the form of widespread changes in the main components with considerable costs and consequently performance improvement, or very limited changes to some minor items with minimum cost. As an optimum solution, achieving higher performance with increasing TIT [1], along with improved life and maintenance intervals, was determined as the main scope of upgrade for the new version MGT-70(4).

To achieve the desired increase in performance parameters, it was decided that the baseload TIT be increased from 1090 °C in MGT-70(3), to the target value of 1105 °C in MGT-70(4), with which gas turbine cycle calculations predict an increase of approximately 4.5-5 MW in turbine output power and a corresponding efficiency improvement of around 0.1% compared to the MGT-70(3) generation. The reason for not choosing a higher TIT is to avoid the need for additional modifications to the main rotary parts and casings and as a result, limit the replacement to the very first three rows of blading (Vane Row 1, Blade Row 1 and Vane Row 2). This targeted approach enables a swift implementation during a scheduled HGPI (Hot Gas Path Inspection) procedure, minimizing downtime and ensuring efficient maintenance.

Beyond enhancements to GT performance, the upgraded machine has been designed with a focus on extending its maintenance interval compared to its predecessor. In this latest version, the machine can operate for 50,000 EOH in new life-mode conditions before requiring major maintenance, thereby eliminating one major inspection (HGPI) at 100,000 EOH. This reduction in maintenance frequency will have a significant impact on reducing service costs and enhancing availability.

After the main scope of upgrade was specified, detail design phase consisting of all required analyses on all main components of the machine in new working conditions started. For the first step, turbine blade 1, turbine vane 1, and turbine vane 2 were considered for cooling path modification. The cooling system of air-cooled blades was designed and optimized to achieve the best cooling efficiency while reducing production time. To maintain the overall performance characteristics of the machine relative to the previous version, all modifications on the mentioned blades/vanes were restricted to the internal cooling configuration, without any change in airfoil condition.

[1] Turbine Inlet Temperature

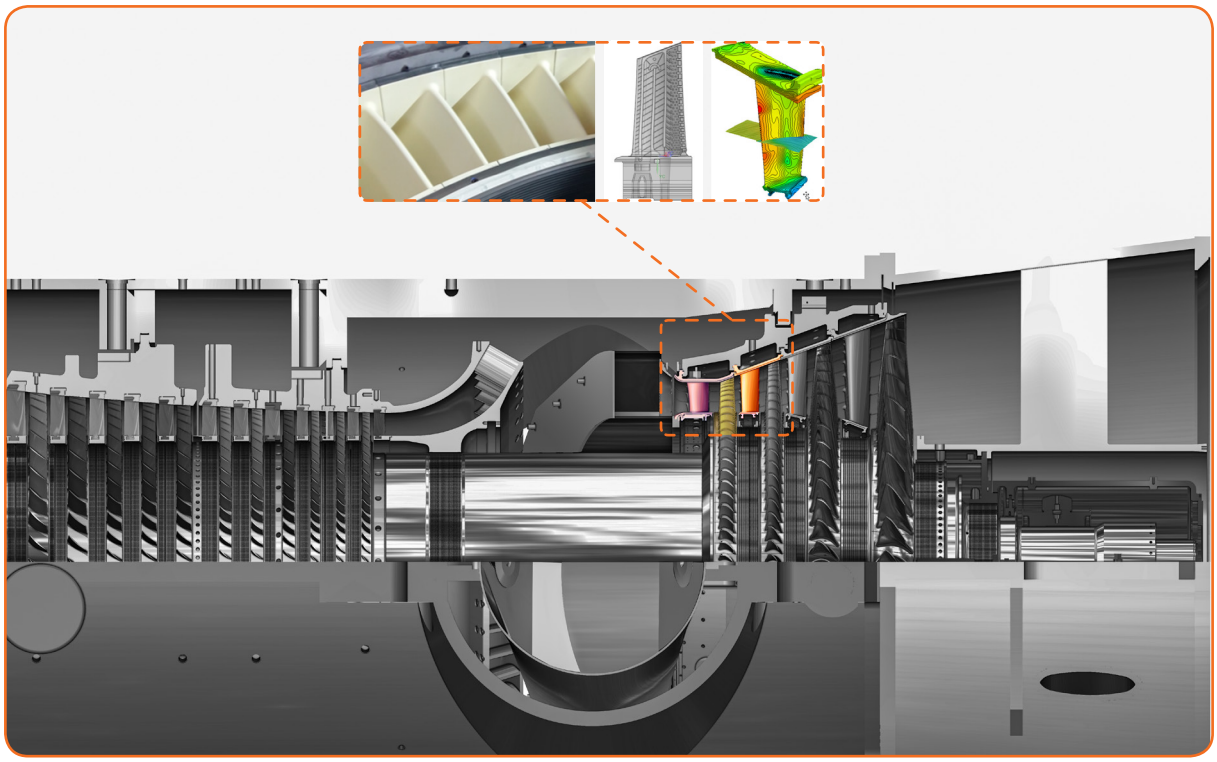

Figure 1 - Modified Parts of Turbine Section

The manufacturing difficulties and requirements were also considered to get minimum geometry complexities. The ceramic core was designed, modified and manufactured based on TUGA's state-of-the-art engineering and PARTO's casting experience to achieve the lowest scrap rate and manufacturing cost.

Next, the manufacturing process for the modified blades/vanes wsa developed and checked by the engineering team of the manufacturing department to detect and rectify any defects in the process. The history of experiences and information gathered from the used parts of the previous versions, especially MGT-70(3), played a key role in this process.

Upgrade Implementation and Commissioning

Prototyping of MGT-70(4) gas turbine was carried out by implementing the modifications on one of the in-service units of previous versions during its overhaul period instead of a whole new machine, to reduce prototyping cost and time. Many issues such as power plant location, environmental conditions, and capacity were considered during the selection of the candidate MGT-70 unit and finally unit 5 of Parand power plant was found to be the most suitable gas turbine for this purpose.

In coordination with the plant owner, plans were made to implement the upgrade during the LTE [2] process. This unit had been upgraded to MGT-70(3) about 4 years ago, and many elements of MGT-70(4) had already been implemented during the previous upgrade.

The overhaul was completed by the end of February 2024. After adequate operating in turning gear mode and the usual subsequent minor inspection of hot components of the unit, as no significant indications were observed during the inspection, normal operation of the unit commenced. After a period of approximately two months, deemed sufficient for operational stabilization, a performance test was conducted to precisely assess the changes

[2] Life Time Extension

in the upgraded unit parameters compared to the previous version. This evaluation aimed to accurately quantify the improvements achieved through the upgrade and validate the expected performance enhancements

According to the predefined operation scenarios, three modes of operation can be considered for this machine that are adjusted in the control system in final tuning of the machine during performance test procedure. Main characteristics of these modes are indicated in the table below.

Table 1 - Operation modes of MGT-70(4) gas turbine

	TIT (°C)	Power (MW)*	Maintenance Interval (EOH)
Base-Mode	1105	190	33,000
Life-Mode	1090	185	41,000
Extra Life-Mode	1075	179	50,000

* Power at generator terminal, corrected to ISO condition, unit aging is considered.

Concluding Remarks

In this article, the comprehensive process of the MGT-70(4) upgrading project was reviewed, tracing its development from the initial examination of various upgrading scenarios to the creation of a project schedule, manufacturing, and implementation of the upgrade in one operational unit. The project's total duration was approximately 3.5 years, encompassing overall and detailed engineering, supply and manufacturing, commissioning, and testing of the upgraded unit.

Following the completion of the detailed design phase and finalization of the necessary procedures, preparations were made for casting of these components to produce the initial batch of the upgraded blades/vanes. Concurrently, investigations were conducted to identify the most suitable unit for the upgrade implementation, ultimately Unit 5 of the Parand Power Plant was selected as the candidate for the upgrade. The upgrade was executed during the LTE period, and the unit was subsequently commissioned. The performance test results indicated a notable increase of approximately 4.5 MW in base load power, as well as an enhancement in base load TIT, as a direct outcome of this upgrade.

2

Developing a Knowledge-based Refurbishment Process for MGT-30 Stationary Blades

Saeedi, Behnaz
Rastar, Vahab
Fathi, Alborz
Mousavipour, Reza
Shahrzad, Saeid

MAPNA Turbine Engineering & Manufacturing Co. (TUGA)

Introduction

According to the design documents of MGT-30 gas turbine, it is essential to inspect, refurbish or replace some critical parts after specific periods of service. Those parts used in hot gas path are important due to high value, especial production processes and high temperature failure mechanisms. On the other hand, due to some technological and metallurgical limitations in production processes, repairing these parts instead of replacing them can bring about high added value.

Turbine blades are subjected to high mechanical and thermal loadings in aggressive and high-temperature environments. All these mechanisms reduce the mechanical and aerodynamic integrity of the blades and limit their useful life.

Failure mechanisms in general include oxidation, creep, cracking and dimensional distortion. It is vital that incoming inspections are robust enough to define the ensuing repair scope and identify parts that are beyond repair from the onset properly.

Depending on the nature of the damage, a refurbishment cycle could include welding, brazing, heat treatment, or recoating. These processes can individually and in combination alter the mechanical and metallurgical properties of the vane, and therefore extend the expected life of the repaired component. Before, during and after all these steps, some specific dimensional non-destructive performance tests should be considered to ensure the quality of the final part. In this article, the whole process developed to repair and refurbish the first two stages of stationary hot blades of MGT-30 gas turbines is described. Different sections of the article elaborate on the refurbishment process for the first two stages of stationary blades.

Identification (Damage Assessment)

All the vanes are preliminarily inspected through visual checking to evaluate the general condition of the component and determine the extent of damage (heavy deformation, general damages etc.). The location and extent of the damages including probable repaired area, crack, deformation, chipping, foreign object damage, oxidation, surface erosion or coating loss are recorded.

Incoming Inspection

The coating is completely removed by proper method. Regarding the chemical composition of the coating and base material, the removal method is selected for each set of vanes. The cooling passages and uncoated areas are masked with appropriate material. It is very important to note that the base material should not be destroyed during the coating removal process.

After coat stripping, the components are visually inspected after heat tint process to ensure that the coating has been completely removed. A clean surface will look evenly dark blue to black, while coating will show up as silver to gold, and any other discoloration could indicate contamination. In case we encounter residual coating, the process of coat stripping shall be repeated.

Metallurgical Evaluation

Turbine vanes and blades are exposed to hot gas for a long time and various changes could occur in their metallurgical microstructure. This metallurgical degradation impairs mechanical properties.

Microstructure degradation includes changes in the shape of gamma prime, not being in cubic form, coarsening and dissolution of gamma primes, connection of carbides and formation of TCP phase, etc. Each of these structural changes can activate destructive mechanisms such as creep, fatigue or thermal fatigue. Figure 1 shows structural degradation of nickel based super alloy turbine vanes after a notable service time.

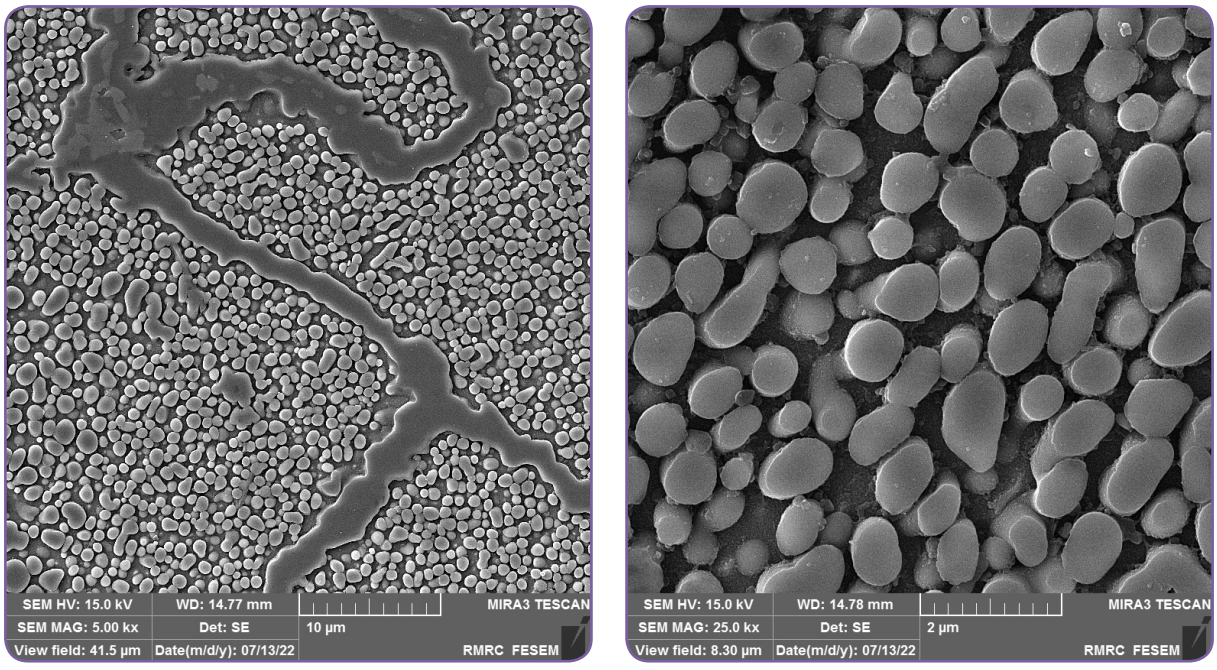

Figure 1 - Microstructure of turbine vane after notable service time

In the process of repair, in order to prevent the destructive mechanisms from being activated, the rejuvenation heat treatment should be performed in the best possible way. This process is usually implemented in one or more stage cycles, depending on the conditions of chemical composition, structure and service history.

In the project at hand, optimized cycles of thermal operation with proper sequence considering the repair and coating requirements, were specified and performed for both vane stages.

Repair Process

As previously described, different areas of the vanes were visually inspected and tested by fluorescent penetrant, after coat stripping and cleaning. All existing defects such as cracks, erosions, pits, geometrical deformations, etc. were identified and recorded. Figure 2 shows nozzle vanes after FPI.

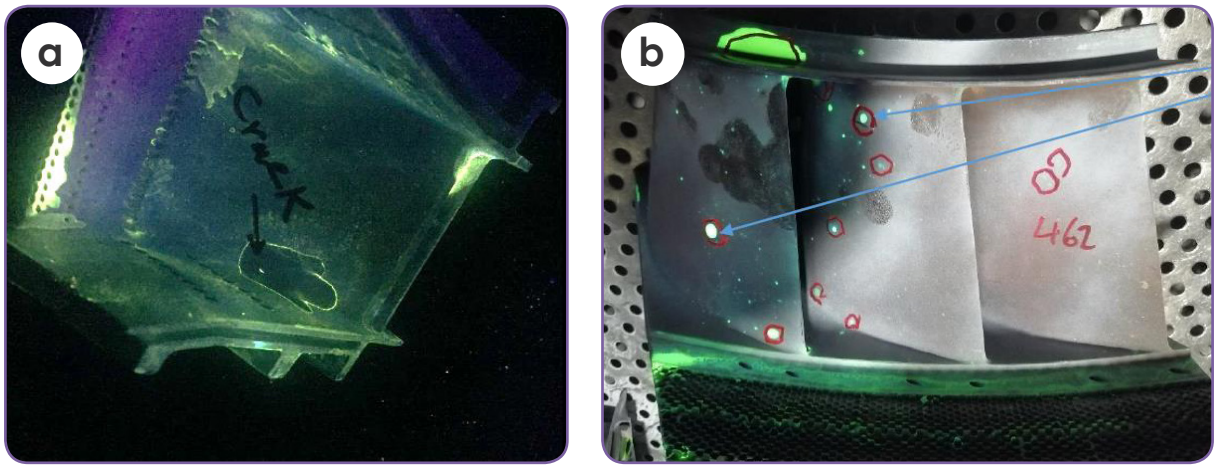

Figure 2 - Inspection and defect identification on MGT-30 nozzle vanes by FPI
a) 1st stage nozzle vane, b) 2nd stage nozzle vane

It is necessary to mention that the 2nd stage nozzle vanes have honeycomb seals which were damaged due to their operation. Figure 3 shows an example of such damaged seals. Due to severe damage to the honeycomb seals, they were removed by machining to be replaced with new ones in the repair process.

Figure 3 - Honeycomb seal area on a 2nd stage nozzle vane of MGT-30 after first overhaul duration

All identified defects were removed by grinding and other proper methods and then inspected using FPI again in order to ensure that defects were completely removed. Figure 4 shows the 1st stage nozzle vane of MGT-30 after defect removal by grinding.

Figure 4 - A 1st stage nozzle vane of MGT-30 after defect removal by grinding

Defects on places other than airfoils, were repaired by a proper filler wire through GTAW process using approved WPS according to BS EN ISO 15614 standard. Figure 5 shows some areas repaired by GTAW welding on MGT-30 nozzle vanes.

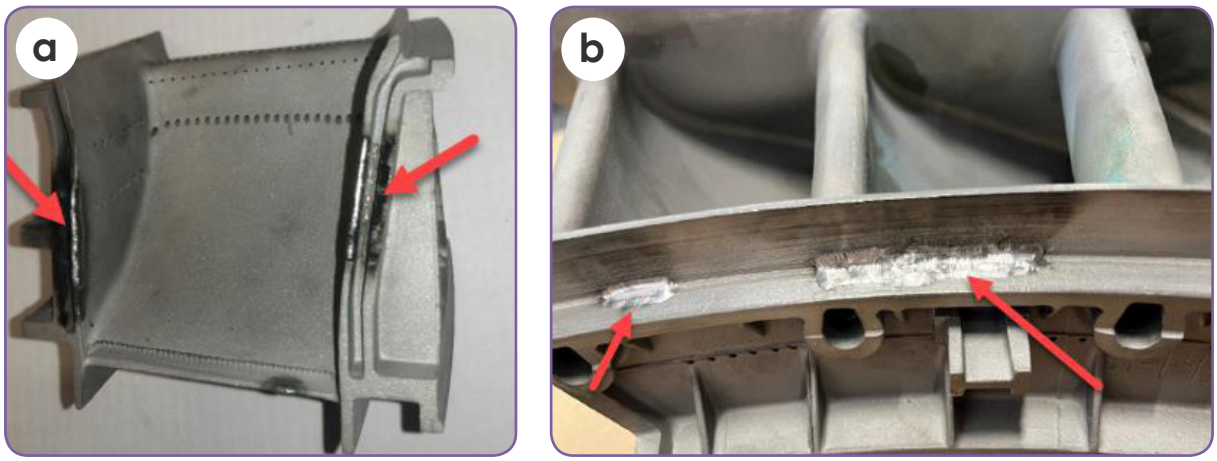

Figure 5 - Areas on MGT-30 nozzle vanes repaired by GTAW process
a) 1st stage nozzle vane, b) 2nd stage nozzle vane

Due to the sensitivity of the airfoil areas and the high risk of cracking, it was more preferable to use a process with very low input heat to repair the defects in these areas. Therefore, defects on the airfoils were repaired through Laser Beam Welding (LBW) using a nickel based wire, with a qualified WPS according to BS EN ISO 15614 standard. Welded areas were ground and then inspected both visually and making use of Fluorescent Penetrant Inspection (FPI) to ensure the absence of defects. Figure 6 shows some areas repaired by LBW on airfoil areas of the nozzle vanes.

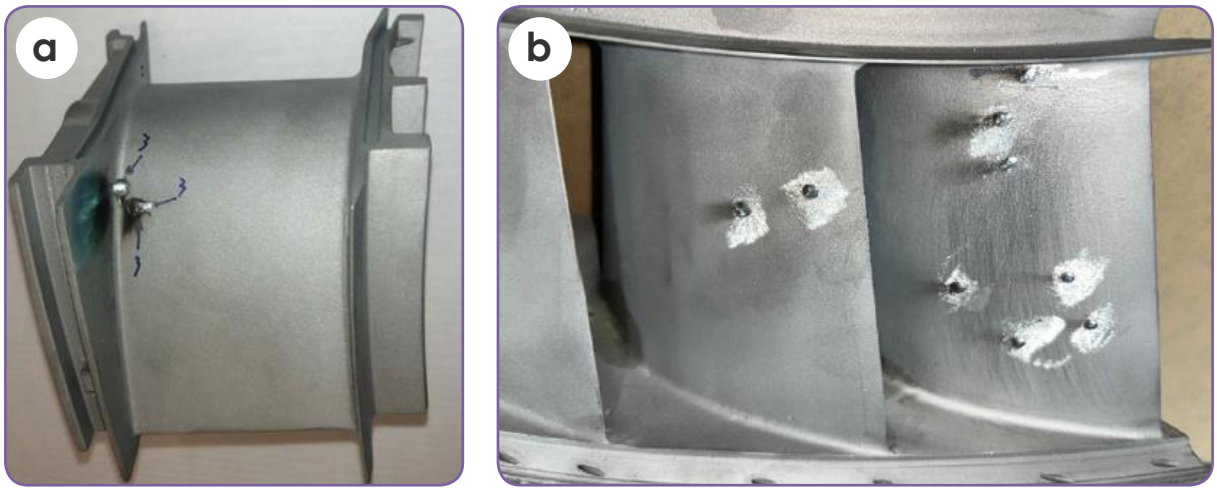

Figure 6 - Repaired areas on MGT-30 nozzle vanes by LBW process
a) 1st stage nozzle vane, b) 2nd stage nozzle vane

As mentioned earlier, the honeycomb seals of 2nd stage nozzle vanes usually should be replaced.

Thus, honeycomb seals made of solid solution nickel base super alloy, in accordance with the drawing dimensions, were brazed to 2nd stage nozzle vane bodies. Brazing was done in the vacuum furnace using approved procedure according to AWS C3.6 standard.

First, honeycomb segments were degreased by acetone before brazing and then installed using resistance tack welding. A suitable filler metal according to AWS A5.8 was applied with the help of a brush inside of the segments with evenly thin layer. Finally, the brazing thermal cycle was applied to join the honeycombs in a vacuum furnace.

Visual inspection was performed to check the brazing quality of the honeycomb elements interconnection and brazing to the part base around the edges/perimeter. The brazing quality was satisfactory because the braze material had fused and there was a fillet around the edges/perimeter of the honeycomb element. Figure 7 shows a 2nd stage nozzle vane of MGT-30 after replacing the honeycomb seal.

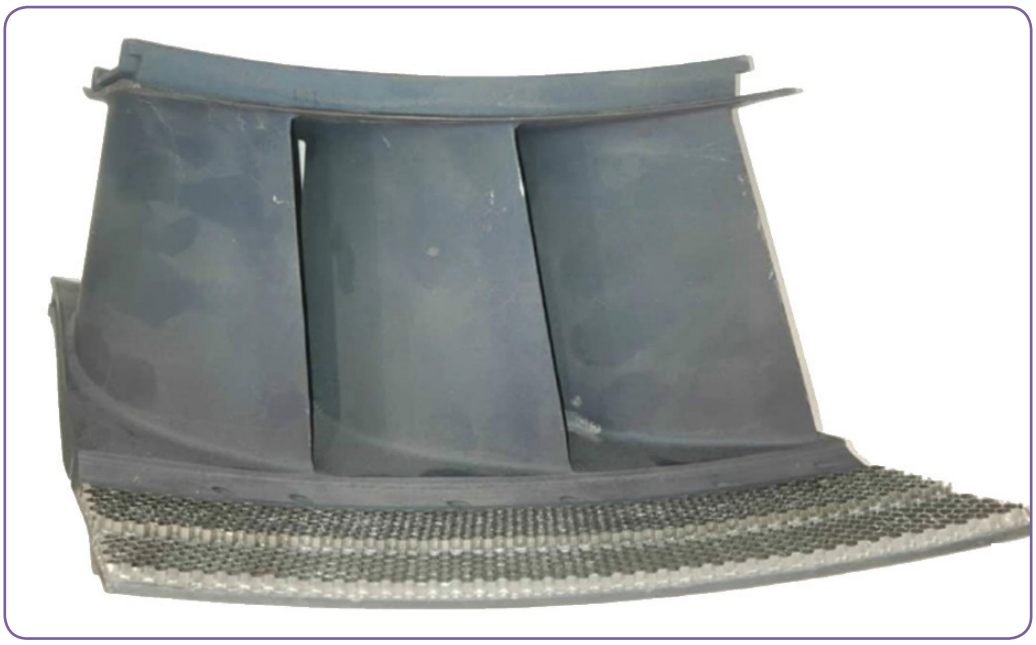

Figure 7 - A 2nd stage nozzle vane of MGT-30 after replacing honeycomb seal

Coating

After the repair process, the new coating could be reapplied on the components. All requirements for coating process, including powder material, coating application processes & parameters, and supplier qualification were checked and approved before starting the process.

Coating process verification was carried out by means of pre-production test pieces. Since coating a flat test piece may significantly differ from coating surfaces with complex geometries, it was essential that coatings are also applied on the actual test components. Thus, verification process was performed in two steps consisting of coating and subsequent quality assurance testing of flat specimens and scrapped vanes. Coated test coupons at the critical points on the scraped vane were destructively evaluated. Metallurgical inspection revealed thickness, interface contamination, oxides (in metallic bond coat of TBC), porosity, un-melted particles, cracks, roughness and any other contamination and inclusion.

After cleaning, the surface was roughened by white alumina grit blasting for the 1st stage nozzle vane coating. MCrAlY bond and YSZ top coat were applied with Air Plasma Spray (APS) method. TBC quality control items included surface condition (Visual inspection), bend test, bond strength test, MCrAlY and YSZ layers microstructure with metallographic inspection (Figure 8).

To ensure that the final coated part is serviceable, non-destructive testing and dimensional checking were carried out. In terms of visual inspection, there shall be no chips, discontinuities, flaking or cracks in the coating system with complete uniformity. Any embedded particle or irregular surface profile in the coated areas of the component is unacceptable. Moreover, the components were checked for any overspray on the uncoated and incomplete coating areas. Ceramic top coat thickness was measured with an eddy current gage. As every coating specification contains requirements for the final surface quality, polishing was necessary to obtain the specified surface roughness for the current part.

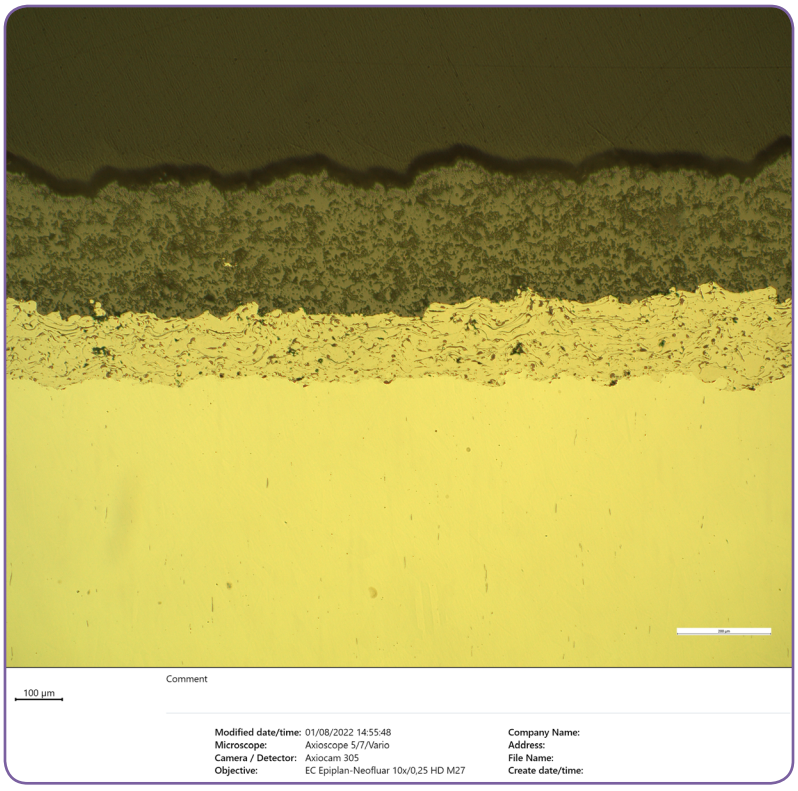

Figure 8 - Microstructure of TBC (MCrAlY/YSZ) on the test pieces

In the 2nd stage nozzle vane coating process, after surface preparation, aluminide diffusion coating was applied using pack cementation process as a protective coating. The cooling passages and uncoated areas were masked with appropriate material.

The activity of Al is maintained at the surface of the substrate and the process temperature defines two categories of deposition methods: high temperature-low activity (HTLA) and low temperature-high activity (LTHA), also referred to as outward and inward diffusion respectively. Using any method shall satisfy the defined quality specifications. For the current parts, LTHA aluminide coating was deployed.

Required inspection and test items for applied aluminide coating on the test pieces, scrapped vanes and the main parts include coating material, surface condition, coating microstructure, thickness, surface roughness, aluminum content and phase analysis. All the items were evaluated and accepted in the current set of vanes.

During visual inspection of the test pieces, scrap vanes or the main parts, the surface condition of the coating had a uniform continuous surface, free from blistering, spallation, scratch, chipping, cracking, discoloration and other visual imperfections. Moreover, on the main parts, the applied coating covered all surfaces according to the relevant drawing of the vanes. A fine blasting was also performed on the final surface of the parts to achieve an approved roughness.

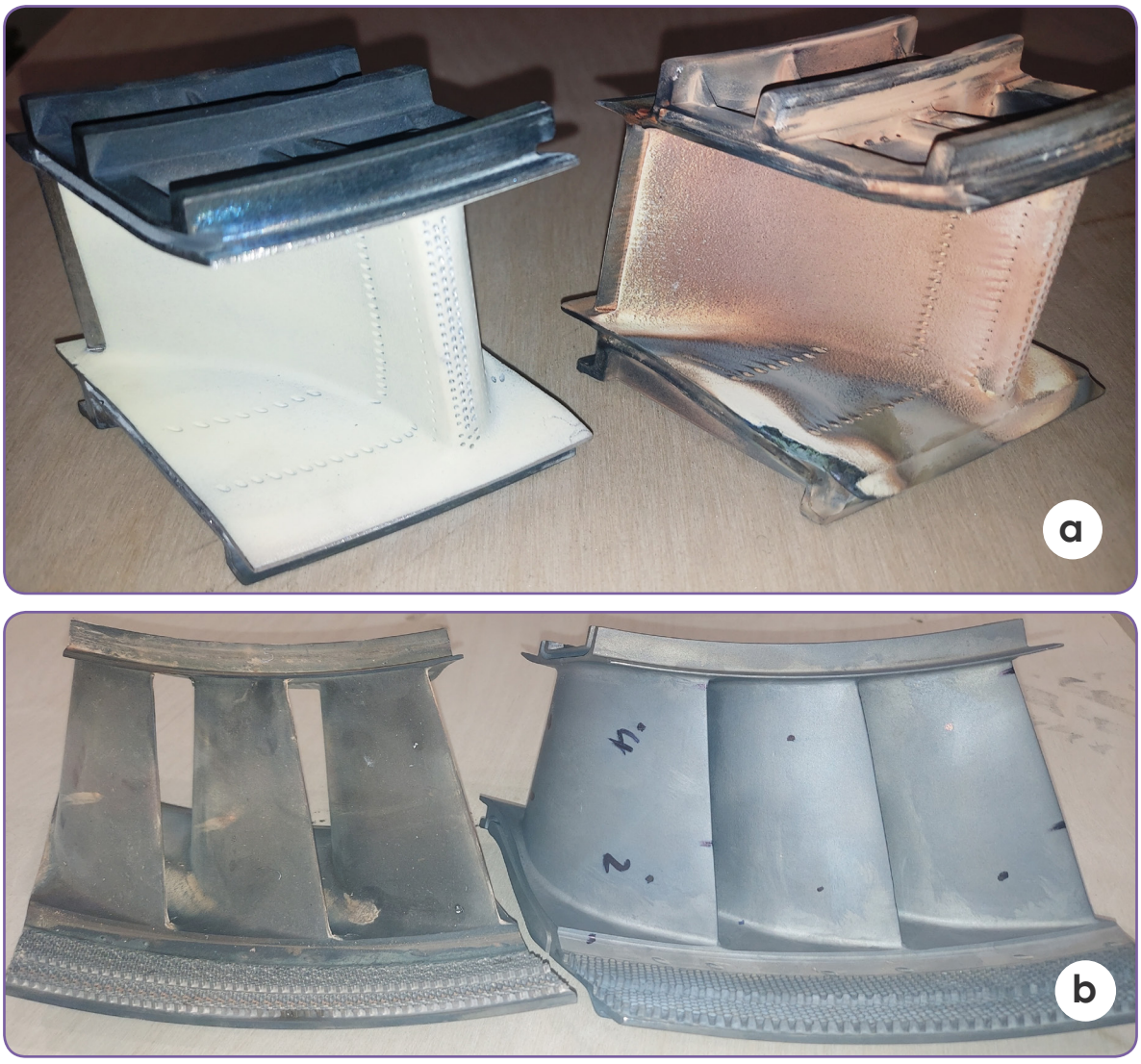

Figure 9 - a) First and b) second stage nozzle vane before and after repair

Since only visual inspection and roughness measurement of the coating were performed on the final parts, to evaluate the coating more accurately, several test pieces were aluminized and heat treated along with the main parts, as controlling samples per each batch. The samples were then destructively evaluated. The samples were mounted on the critical points of the main parts.

Metallographic evaluation on the prepared cross section of the coated test pieces revealed the microstructure and thickness of the coating. Aluminum content and β-phase in the surface and regions near the relevant test pieces were analyzed via SEM equipped with EDS and XRD, respectively. The results show that these parameters are within the accepted range.

Since the coating procedures used included relatively high temperature processing, it was checked in a complete heat treatment cycle. Heating cycles in the coating process shall ensure that properties and microstructure of the base metal are not impaired.

At the end of the coating process, heat tinting was carried out to ensure the coating had been completely applied on the vane surface. The coated surface is seen as silver to gold.

A first and a second stage nozzle vane before and after the coating process are shown in Figure 9.

Dimensional Check

The accuracy of the dimensions of the nozzle vanes directly impacts the performance of the gas turbine. Any deviations in dimensions can affect the aerodynamics and flow characteristics of the turbine, resulting in reduced efficiency, performance, output power, and increased fuel consumption. Dimensional checks are also crucial for assessing the structural integrity of the nozzle vanes. Deformations, cracks, or distortions can compromise the strength and functionality of the vanes. Therefore, conducting dimensional checks of the key features and areas is essential for maintaining optimal performance, identifying erosion or wear, ensuring structural integrity, and adhering to design specifications. After the repair process, the following geometrical features and dimensions were examined during this project:

1. Vane Profile: The shape and contour of the vanes were inspected to ensure that they meet the original design specifications. Any deviation can impact the gas flow and turbine performance.
2. Vane Thickness: The thickness of the vanes at different sections was measured to ensure that it fell within an acceptable range. Excessive erosion or corrosion can lead to thinning of the vanes, compromising their structural integrity.
3. Vane Gap: The clearance between adjacent vanes was measured to ensure that it fell within the specified range. An excessive gap can result in hot gas leakage, reducing turbine efficiency.
4. Vane Twist: The twist angle of the vanes along their length was checked to ensure that it matched the original design. Any deviation can affect gas flow and turbine performance.
5. Vane Leading and Trailing Edges: The leading and trailing edges of the vanes were inspected for signs of erosion, cracking, or damage. These edges are critical for maintaining gas flow and coolant flow and should be in good condition.
6. Vane Cooling Holes: The cooling holes in the vanes were inspected for blockages or erosion. These holes are essential for cooling the vanes and preventing overheating.
7. Vane Mounting: The attachment points of the vanes to the turbine casing or rotor were inspected for signs of wear, cracking, or misalignment. Proper mounting is crucial for maintaining the position of the vane and structural integrity.

In cases of significant geometrical deviations, a comprehensive FEM/CFD analysis was conducted to evaluate the resulting effects on the flow path and structural integrity.

Air flow & Water flow

In addition to inspecting the aforementioned geometrical features and dimensions, air and water flow tests through the cooling passages and vane holes are crucial during the repair process and life extension of the hot section nozzle vanes of a gas turbine. Insufficient flow can lead to inadequate cooling, while excessive flow can affect overall turbine performance. Any blockages, geometrical restrictions, or imbalances can result in uneven cooling and potential hot spots. Conducting air and water flow tests helps ensure the effectiveness of the cooling system and prevents the vane from overheating. In this case, all vanes were installed in a customized test stand to measure the flow rate, ensuring design requirements (Figure 10). Additionally, water flow tests were conducted for all the vanes undergoing repair and life extension, to ensure that the cooling medium is evenly distributed across all holes of a vane.

Figure 10 - Examination of the cooling flow path for 2nd stage nozzle vane using water flow test and radiographic testing (RT)

Concluding Remarks

Production challenges, market trends and sanction issues have led to an increased need to expand technical knowledge for repair and refurbishment of the nozzle vanes of MGT-30 gas turbines instead of replacing them. In this study, failure mechanisms and required steps of refurbishment process were outlined for the first two stages of stationary hot blades. After this research project, it can be claimed that it is possible to return a large percentage of the two first nozzle vanes to another service cycle. It could reduce the final costs in comparison with the supply of new components and help the manufacturer meet annual turbine production schedules.

3

Development of a Precise Spray Measurement System Based on DIA Technique

Akbari, Mohammadjavad
Ranjbaran, Alireza

MAPNA Turbine Engineering & Manufacturing Co. (TUGA)

Introduction

The spray process is widely used in various industrial applications, including chemical, agricultural, pharmaceuticals, as well as propulsion systems, particularly in gas turbines. In the liquid fuel injection process, the droplet diameter distribution significantly influences fuel evaporation, combustion processes, and pollutant level. Therefore, the experimental measurement of spray parameters such as droplets' size and distribution is an integral part of theoretical and empirical investigations regarding the combustion system and fuel oil burner design.

Several optical-based techniques such as Phase Doppler Anemometry (PDA), Laser Diffraction Analysis (LDA), and Digital Image Analysis (DIA) [1-3] are currently employed to measure the diameter of spray droplets. Among these methods, the Digital Image Analysis (DIA) stands out as a cost-effective, straightforward, and accurate technique, which has garnered significant attention from both research and industrial centers seeking to investigate spray characteristics.

Regarding the need for spray analysis and measuring the corresponding parameters in design projects, development of a proper measurement system was planned, and the initial phase involving a simple shadowing setup was performed to identify the spray characteristics, utilizing a pulsed LED light source as described in TR. No.4. In fact, the study demonstrated the effectiveness of a laboratory scale shadowgraph using affordable and uncomplicated pieces of equipment. However, limitations in the required equipment and data processing software hindered its industrial application, particularly for measuring droplet diameter of dense fuel oil sprays.

Accordingly, the main objective of this project is to develop the Digital Image Analysis (DIA) method for precise diameter measurement of spray droplets produced by the liquid fuel injectors within TUGA. This report provides comprehensive insights into the theoretical aspect of the DIA method, the essential equipment required to accomplish it, the calibration process employed, and details regarding the software developed to extract droplet distribution information from the spray.

Theory and Equipment

The DIA method relies on direct imaging employing the spray shadowgraphy technique. The principle involves illuminating the medium from behind, causing the shadow of obstacles between the light source and the camera to be projected onto a camera sensor. Overall, this approach is well-suited for applications where the objective is to examine a transparent medium, containing particles with a high refractive index. This method is notably non-intrusive and does not require physical information about droplets. This technique stands out as a simpler and more cost-efficient one compared to other methods, as it does not require an expensive laser light source. A significant advantage over conventional PDA and LDA methods is its capability to assess the size, shape, and velocity of non-spherical particles.

This technique comprises two essential components: a light source and a camera. In contrast with lasers, the LED light source enables volumetric illumination. To obtain flat and high-quality images, the imaging section necessitates a macro lens with a low Depth of Field (DOF). For capturing spray phenomena, a high-speed digital camera is employed as the detector.

The LED light source and synchronizer were supplied by ARSIN Company. To achieve coinciding operation, the light source signal is precisely aligned with the camera's exposure timeframe using the synchronizer unit. The equipment pieces for the light source and synchronizer are shown in Figure 1(a). The high-speed camera selected for this project is the CB160MG-LX-X8G3 model, manufactured by XIMEA. This camera gives a maximum resolution of 4704 x 3424 pixels and its frame rate at maximum resolution is 311 fps. Also, the Canon EF 180mm f/3.5L Macro USM lens is utilized in this setup. At a minimum working distance of 24 cm, the lens offers a 1:1 magnification, signifying a life-size representation of the object. The camera and lens can be seen in Figure 1(b).

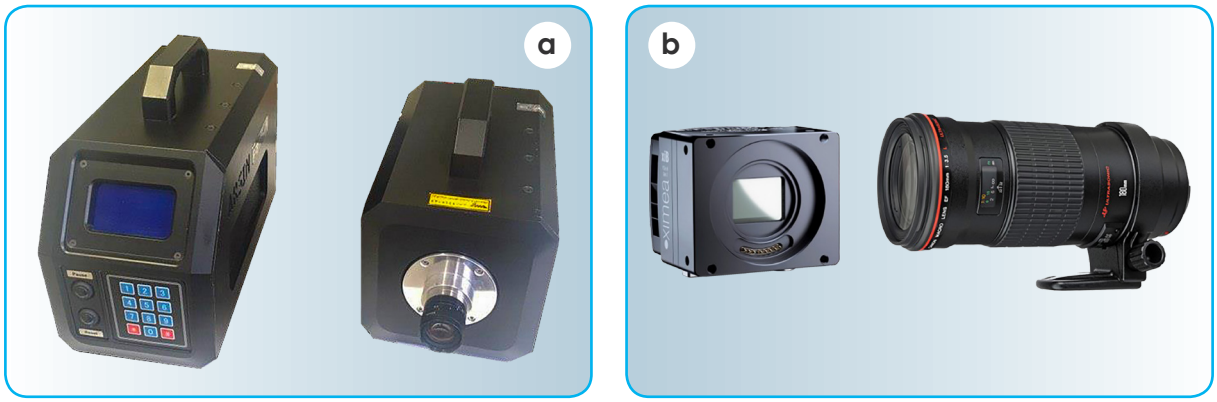

Figure 1 - a) Synchronizer and light source equipment, b) Camera and lens

Out-of-focus Effect and Calibration

In shadowgraphy, when an object is precisely positioned at the imaging system's focus plane, it produces a sharp shadow image on the camera sensor, as illustrated in Figure 2. However, as the target object moves away from the focus plane in any direction, the shadow image on

the sensor becomes blurred, leading to a reduction in sharpness. This phenomenon is referred to as the "out-of-focus" effect. The Depth of Field (DOF) is the range of distances between the nearest and farthest positions of the droplet from the focus plane, where acceptable sharpness is achieved on the sensor plane.

In real situations, spray droplets are positioned at various distances from the focus plane. To accurately estimate spray droplet size, it is crucial to address the out-of-focus effect for droplets of different sizes. This is a significant step in the calibration process. This process includes the steps of capturing droplet images with a different size at several distances from the focus plane, and providing methods for estimating the droplet size using image processing techniques.

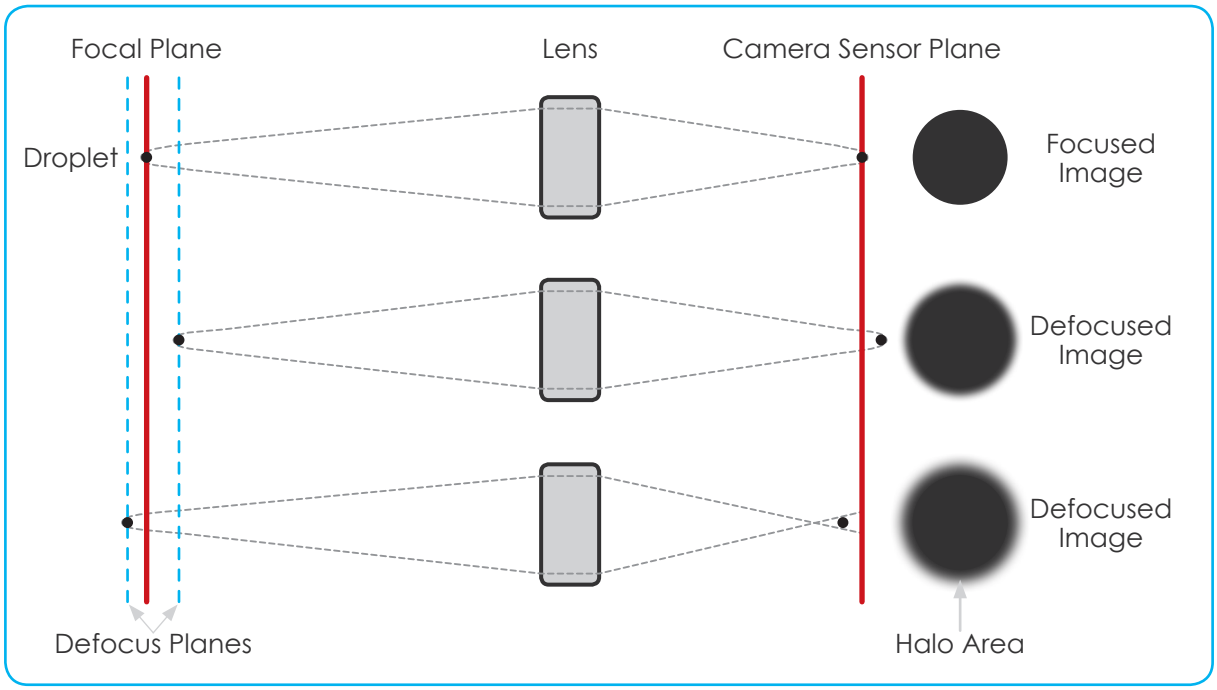

Figure 2 - Schematic of the drop in Focus and Defocus position of the imaging system and the resulting image

In this study, a calibration slide comprising optical slides with two-dimensional circular sections of specific dimensions is employed. The initial phase of the calibration process involves capturing images of the calibration slide at 60 distinct points. Multiple techniques have been introduced to address the out-of-focus concern, and the approach proposed by Senthilkumar et al., [4] is adopted for this work. This phase comprises several sequential procedures, with each step being executed through MATLAB, as illustrated in Figure 3. By employing a specific threshold on the processed image, a binary image is generated. Subsequently, the area and equivalent diameter of the droplets are extracted in pixels using this binary image.

For measuring the droplet diameter under out-of-focus conditions, two thresholds, namely the upper and lower thresholds, are applied to the image. Based on these thresholds, two areas (upper area and lower area) are extracted for each droplet. The equivalent diameter is then calculated as follows:

$$d_{drop} = \sqrt{\frac{2(Higher\ threshold\ area + lower\ threshold\ area)}{\pi}} \quad (1)$$

The selection of the thresholds is of utmost importance to minimize the diameter calculation error. During the calibration process, increasing the distance between the calibration slide and the focus plane leads to a proportional rise in droplet blurriness. As a result, the corresponding proportion of the area derived from the upper and lower thresholds also increases.

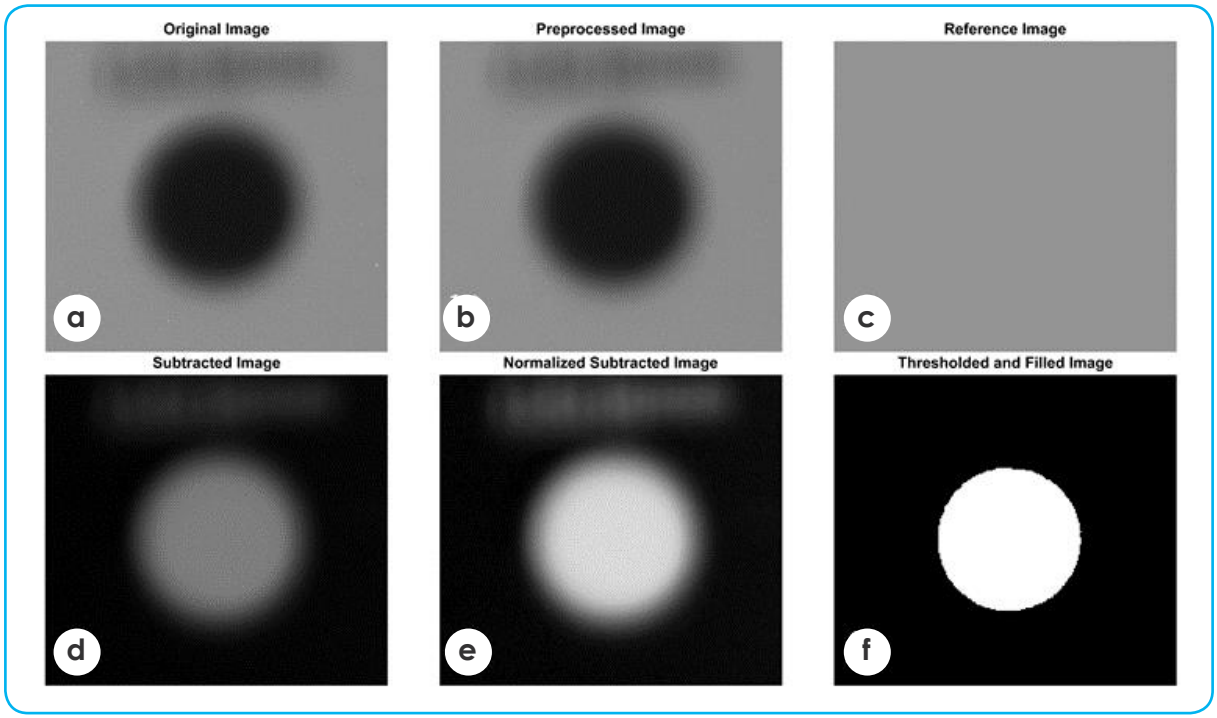

Figure 3 - Image processing steps to extract droplet diameter. A full circle with a diameter of 508 microns at 1.9 mm from the focus plane.
a) raw image, b) filtered image, c) background image, d) removal of background effect, e) normalized image, f) binary image with 62% threshold applied

Figure 4 depicts variations in the area ratio alongside the error of the equivalent diameter calculation through equation (1), against the distance of the calibration slide from the focal plane for a complete circle with a 254-micron diameter. This Figure shows that the sharpest state is achieved at the focus plane, which corresponds to the lowest area ratio. As the distance from the focus plane increases, both the area ratio and the corresponding error experience almost linear increment on both sides. This observed trend of changes in the area ratio and error validates the viability of the model for accepting out-of-focus droplets detected in real images. Considering an area ratio acceptance limit of 1.2, the maximum error resulting from measuring a full circle with a 254-micron diameter is about 3%, which is a highly favorable value.

The calibration process involves the evaluation of all full circles on the calibration slide. After conducting a comprehensive analysis of all the collected data, it has been determined that by setting the upper, lower, and global threshold values to 62, 70, and 52, respectively, and additionally selecting an area ratio limit of 1.2 to accept out-of-focus droplets, the maximum error resulting from post-processing remains below 5%.

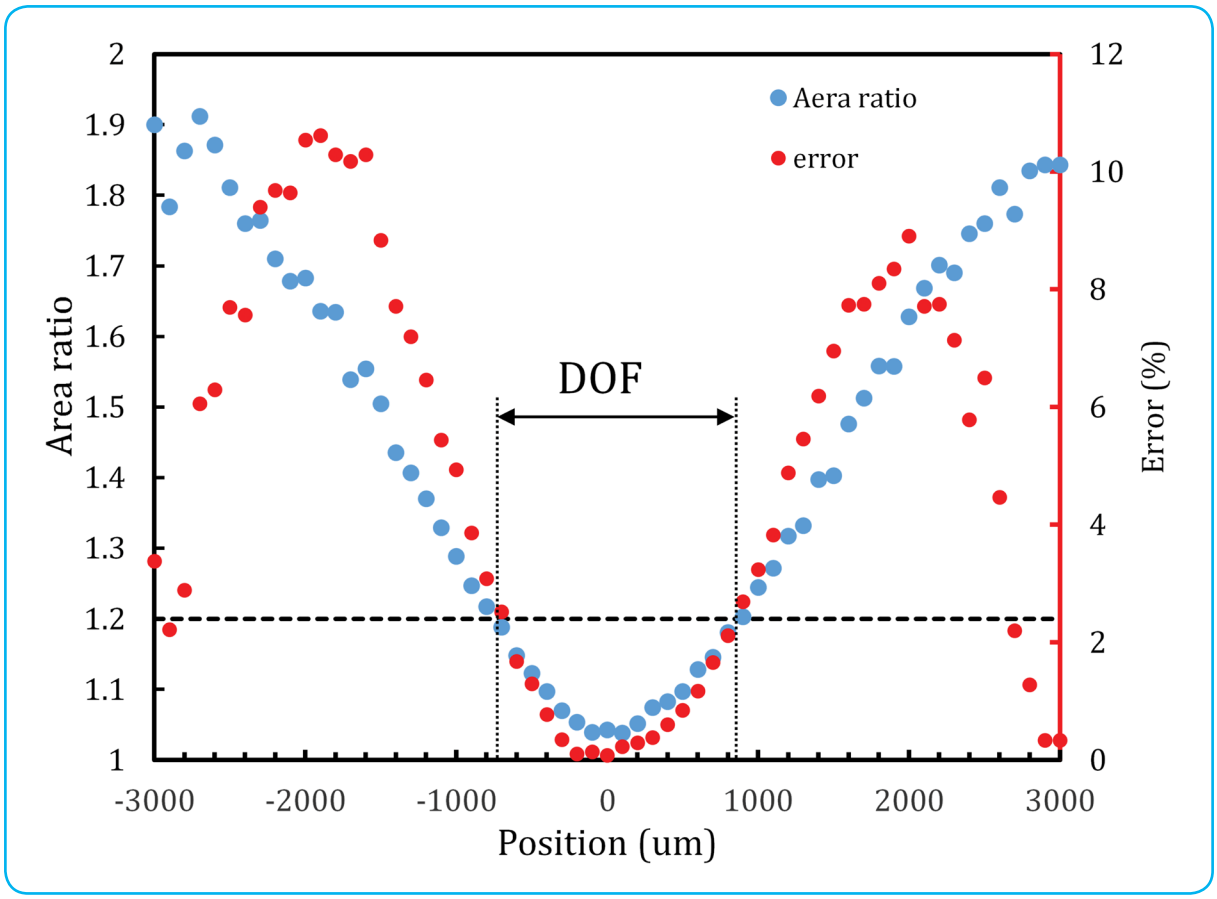

Figure 4 - Changes in the area ratio of the lower and upper threshold and the corresponding error according to the distance of the calibration slide from the focal plane (Full circle diameter: 254 microns, Upper threshold: 70%, Lower threshold: 52%)

An Industrial Gas Turbine Fuel Oil Spray Droplet Measurement

In this section, the DIA method is employed for measuring the diameter of a fuel oil burner's spray droplets as part of a real sample test. To do this, a step-by-step procedure was followed. Initially, the camera and LED were interconnected. Subsequently, the LED's light pulse width was adjusted and the intensity level was set to 80%. The pressure behind the injector was set on operating value resulting in a real spray pattern. Figure 5(a) illustrates the experimental setup for employing the DIA method and in Figure 5(b), a sample image from the spray, captured under the aforementioned conditions, is shown. It should be noted that more than 200 images were taken during this comprehensive experimental process.

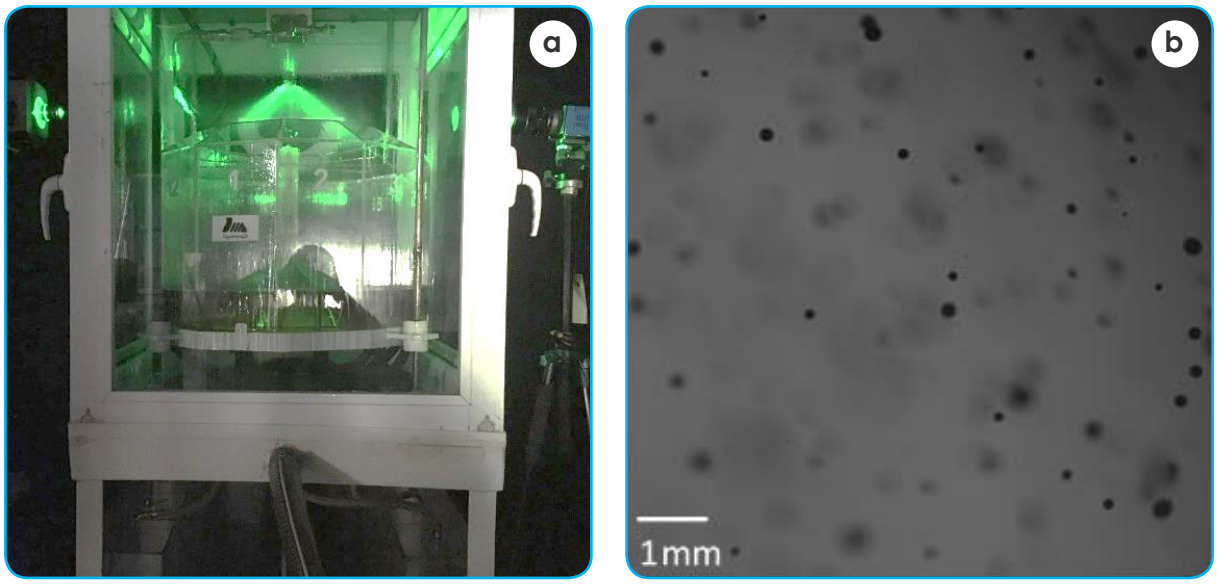

Figure 5 - a) DIA method setup for measuring the L4 injector spray diameter,
b) sample image of L4 nozzle spray droplets at 10 bar pressure

Software Development for Spray Droplet Measurement

To facilitate the utilization of the DIA method, the Spray Droplets Analysis software was developed with the primary objective of extracting the droplet diameter distribution from the spray images. This software offers various pre-processing options, enabling users to specify settings relevant to droplet diameter measurement while effectively correcting out-of-focus errors by selecting their desired area ratio. Moreover, the calibration process necessitates user involvement, where thresholds, minimum droplet area (in pixels), and maximum ellipticity must be carefully selected to accept droplets suitably.

Upon analyzing all the images, the software generates informative output, including a distribution histogram of spray droplets, the average diameter, and SMD value. In a specific test scenario (as depicted in Figure 5(b)), the average diameter and SMD were measured as 134 and 180 microns, respectively, and the extracted distribution exhibited complete consistency with the anticipated theoretical distribution.

To assess the software configurations and potential adjustments, an additional feature enables the preservation of post-processed images. The post-processed image depicted in Figure 6(b) corresponds to Figure 5(b). Specifically, only the droplets contained within colored circles are identified, and among these droplets, only those surrounded by green circles meet the criteria of area ratio, minimum area, and ellipticity filters. Consequently, the green circles are considered for the droplet diameter distribution.

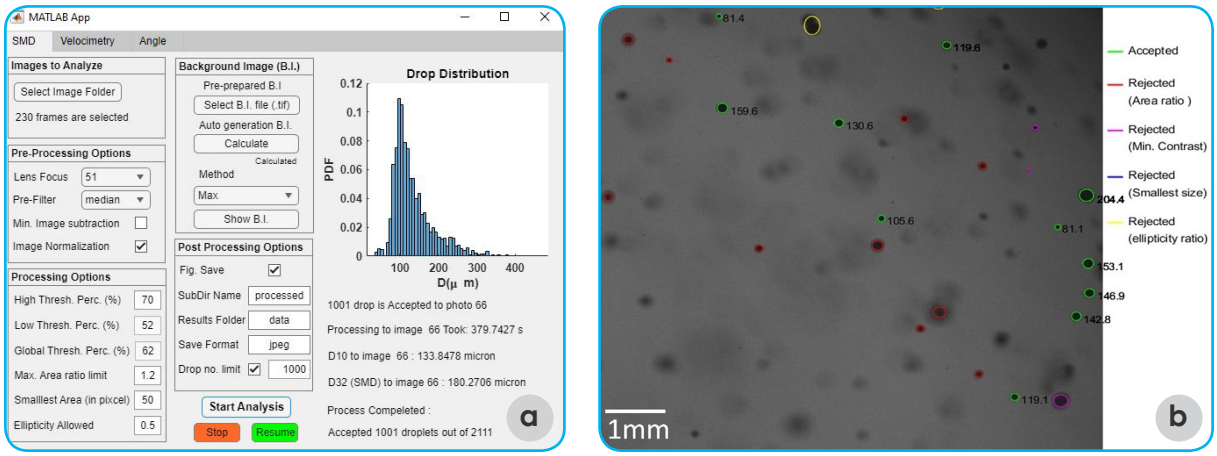

Figure 6 - a) Spray Droplets Analysis software, b) The post-processed image of Figure 10(b)

Concluding Remarks

In this investigation, the DIA (Drop Image Analysis) technique was explored as a prominent optical approach extensively employed for spray droplet diameter measurement, along with its application in advancing the identification tools for combustion chamber laboratories. The calibration process was thoroughly tested and analyzed to correct out-of-focus errors, evaluate methodological uncertainty, accurately calculate pixel-to-micron, and determine important parameters for image processing across different lens conditions and droplet sizes. Subsequently, the DIA method was applied for preliminary tests on an actual GT fuel oil injector. Finally, the Spray Droplets Analysis software was developed to extract droplet diameter distribution and was implemented using the raw test data. The adoption of this method in combustion laboratories represents a simple, cost-effective, and accurate approach that holds significant potential in advancing the knowledge about the design of gas turbine injection systems.

References

[1] Brady, Michael R., Samuel G. Raben, and Pavlos P. Vlachos. *"Methods for digital particle image sizing (DPIS): comparisons and improvements."* Flow Measurement and Instrumentation 20.6 (2009): 207-219.

[2] Brunel, Marc, and Huanhuan Shen. *"Design of ILIDS configurations for droplet characterization."* Particuology 11.2 (2013): 148-157.

[3] Fdida, Nicolas, et al. *"Drop-size measurement techniques applied to gasoline sprays."* Atomization and sprays 20.2 (2010).

[4] Senthilkumar, P., Surendran Mikhil, and T. N. C. Anand. *"Estimation of measurement error and depth of field in PDIA experiments: a comparative study using water droplets and a calibration target."* Measurement Science and Technology 31.11 (2020): 115204.

4

Airflow Test Facility, Accelerating Design and Production

Shaye, Ali
Esmailli, Milad
Ranjbaran, Alireza

MAPNA Turbine Engineering & Manufacturing Co. (TUGA)

Introduction

There are key components in a gas turbine through which flow rates affect the overall performance of the machine. The most important of these components are the burners and turbine blades. The performance of combustion chamber and the gas turbine directly depends on burner's flowrate. In addition, turbine blades without proper cooling passages degrade quickly due to exposure to hot gases. To achieve desired performance, the flow rates in these components must be within limits specified using theoretical calculations and CFD simulations. To ensure that these limits are met, airflow tests are conducted during prototyping and manufacture of the components.

The sample of flow path of TUGA burners and blades are shown in Figure 1.

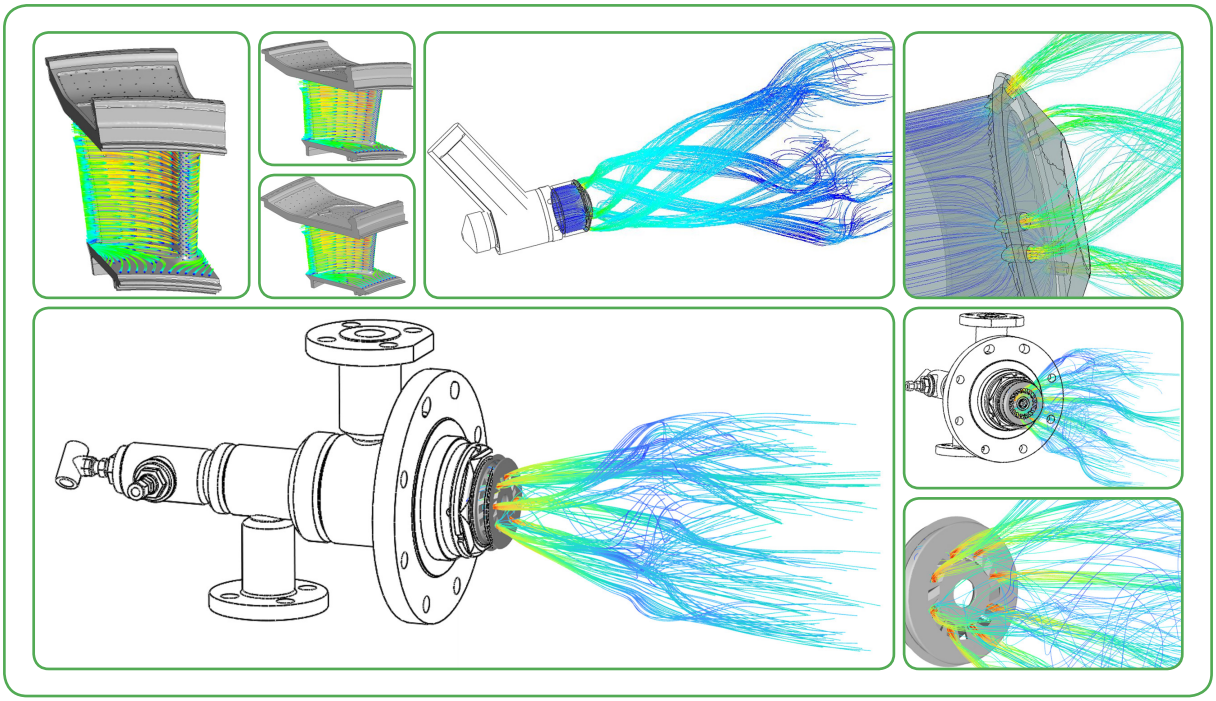

Figure 1 - Flow path and velocity domain in gas turbine components

TUGA's Airflow Test Rig

During the initial stages of development, designers carry out various flow rate tests on prototypes to confirm that the design-specified flow rates are achieved. After completing the design and putting it into production, the flow tests are performed on these components to ensure manufacturing accuracy and product quality.

Consequently, airflow measurement is performed in order to:

- Design new burners and turbine blades
- Verify that manufactured components operate within the design limits
- Determine when repair is needed
- Detect problems such as blocked cooling channels
- Confirm that repaired parts provide performance within design limits (variation in the thickness of the thermal barrier coatings will affect air flow)
- Obtain data for matching components in the final assembly, ensuring consistency and stability

Based on these requirements, the airflow test rig has been designed and fabricated in TUGA. Because of control system facilities and supporting R&D activities, the test bench was established in the combustion laboratory.

As can be seen in Figure 2, the airflow test rig includes an inlet air FRL unit (Filter, Regulator and Lubricator), an electrically actuated on-off valve, an electrically actuated control valve, a high-precision Coriolis flow meter and a stabilizer tank.

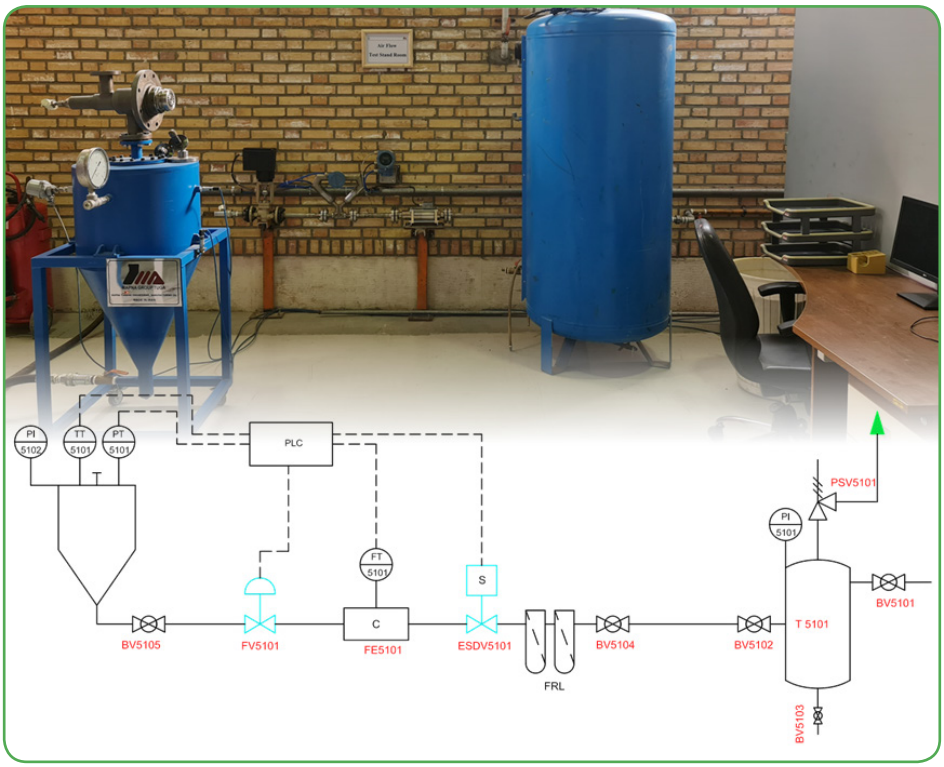

Figure 2 - Airflow test stand PID and components

The PLC based control system considered for the test rig runs with high precision S7-300 controller, enabling a precise control of components and data logging. The particular human machine interface (HMI-Figure 3) enables the operator to configure the system for various tests. Absolute pressure sensors measure the pressure of the inlet and the outlet of the test piece while the pressure ratio is calculated in the control system. A PID controller regulates the control valve to maintain the desired pressure inside the stabilizer tank. After stabilizing the flow, the flow rate is recorded by a high-precision Coriolis flow meter, and the test data is presented in a tabular form. The pressure ratio can be set up to 10 and the capacity of control valve allows testing the components with up to 500 kg/h airflow. These ranges support all TUGA's products that require an airflow test, Such as MGT-20, MGT-30, MGT-40 and MGT-75 gas turbine burners and turbine blades.

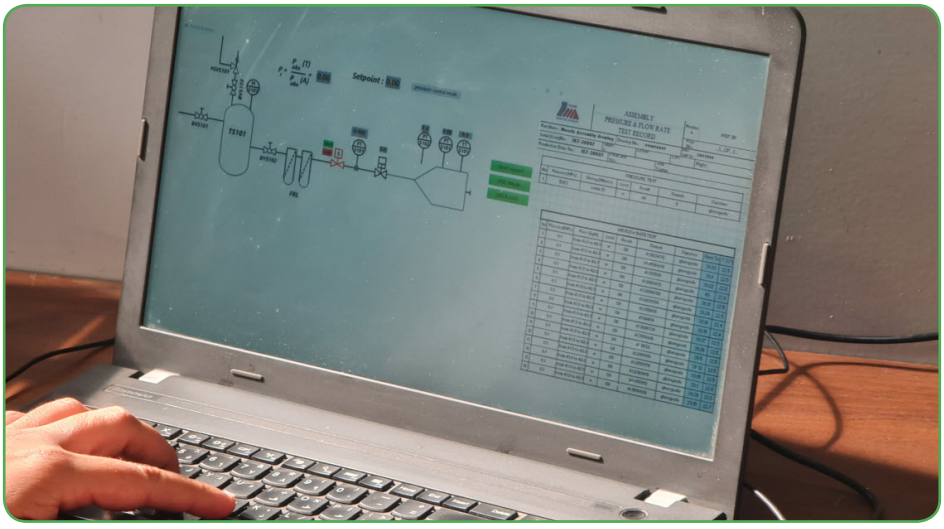

Figure 3 - Airflow test stand user interface program

The flow stabilizer tank is one of the most important components of the airflow test stand. The top part of the tank is specifically prepared for adapter connectors, allowing connecting components and burners with different shapes to the test stand. The tank geometry is designed to ensure reduction in inlet flow velocity and pressure buildup in tank. Flow simulations have been used in the design of the tank to ensure its effectiveness in pressure uniformity and stabilizing. Additionally, after sizing and selecting equipment, the performance of the system was analyzed dynamically for estimating system response time and accuracy (Figure 4).

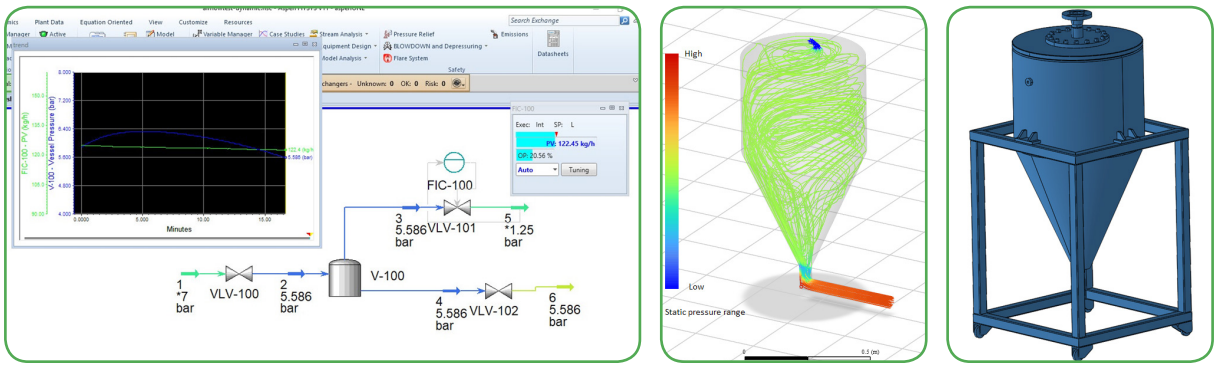

Figure 4 - Design, simulation and analysis of test stand

Concluding Remarks

Establishment and operation of the new airflow test stand in TUGA has provided the capability to test a variety of burners and turbine blades in this company and has led to improvement of the manufacturing process by reducing the cost and time. In addition, this facility accelerates the R&D activities and components production in TUGA. Moreover, the test stand has enabled the company to offer services to other companies requiring airflow tests for gas turbine components (Figure 5).

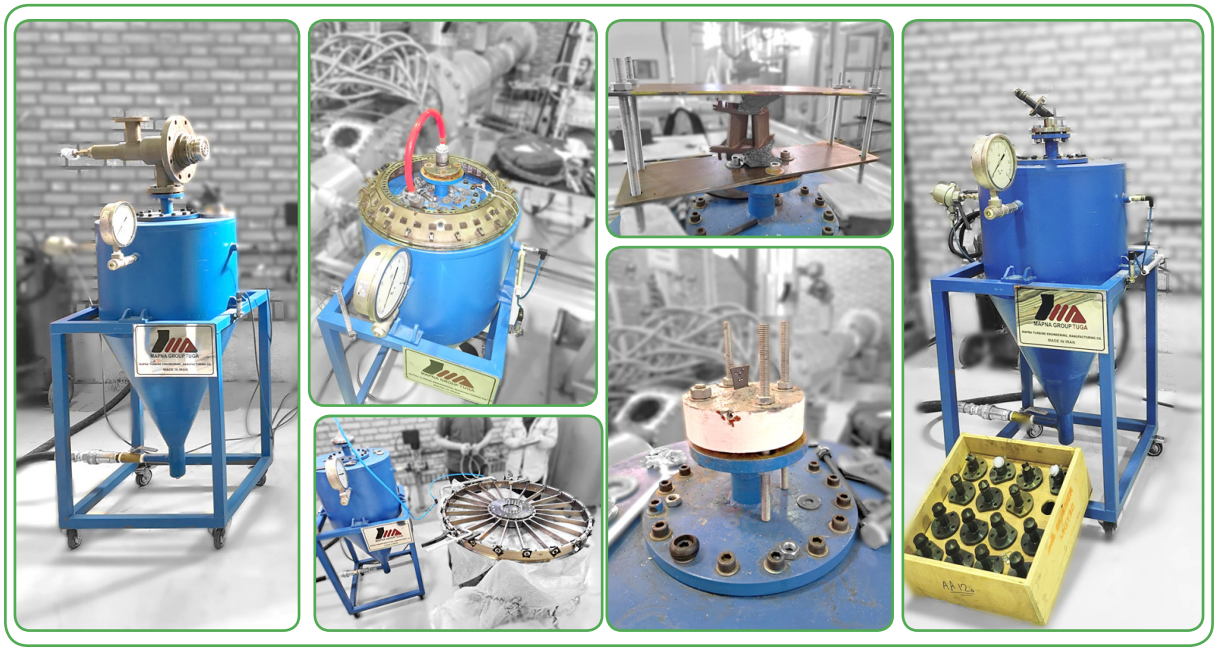

Figure 5 - Various gas turbine components tested in designed airflow test stand

5

An Innovative Method to Characterize Injection Timing of a Diesel Injector and Its Implications for Combustion Studies

Fatemi, Ali
Chehrmonavari, Hamed
akbari, mohammadjavad
Rajabi, Emad
Emami, Arman
Deldar, Hojat

MAPNA Turbine Engineering & Manufacturing Co. (TUGA)

Introduction

As a heavy duty diesel engine developer, a precise identification of the major components and their operating conditions is a necessity for TUGA to provide engineering support, improvement of the performance and durability of products, and modify the application taking into account customer's needs. However, during the early phases of development, these factors are identified using simple engineering tools and in the following steps, analyzed deploying more advanced tools and detailed design methods, and thereby a far-reaching change in the base engine product is gradually made. The injector characteristic, as the first controlling element at the start of the working cycle, affects the establishment of the combustion and consequently impacts the design of other engine components, e.g. the profile of forces imposed on the crankshaft bearings. New generation of fuel injection systems also have the capability to vary injection rate and shape which can significantly optimize the combustion procedure, highlighting the importance of injection characterization. In this article we present an innovative, cost-effective experimental procedure to obtain the injection time characteristics of a high-pressure diesel injector.

Injection Timing

■ Injection delay time

Understanding the exact time of injected fuel plays a pivotal role in simulation of the engine in-cylinder phenomena. The spray formation and consecutive events such as break-up, evaporation, combustion, engine-out emissions are all affected by the injection timing. What engine manufacturers really know is the energizing time of the injector from the engine control unit (ECU). Energizing time is defined as when the ECU generates the injection pulse via an electric command signal and applies it to the coil of solenoid. The duration of this electric command begins with the opening section to act upon actuating a control valve and then triggering the needle to lift, and the closing section returning the needle. The delay time between the electric command and the actual mechanical effect is measured as the injection delay. For a better explanation, Figure 1 depicts the dynamic chain from the signal to the fuel injection, representing the injection delay.

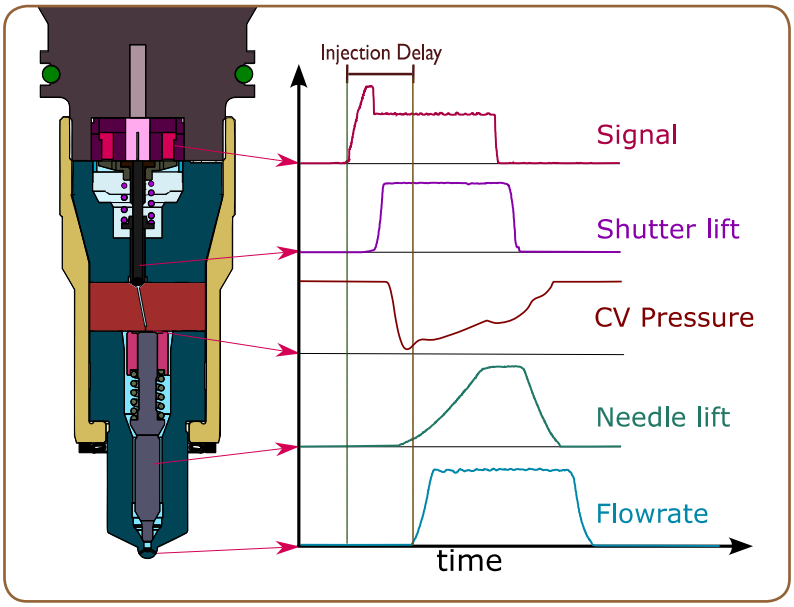

Figure 1 - Solenoid injector dynamic phenomena

■ Causality of delay in injector structure

In order to realize the reasons behind the delay, the behavior of each internal component of the injector should be clarified. In a solenoid common-rail injector, the operational sequence consists of the following chain shown at a glance in Figure 2.

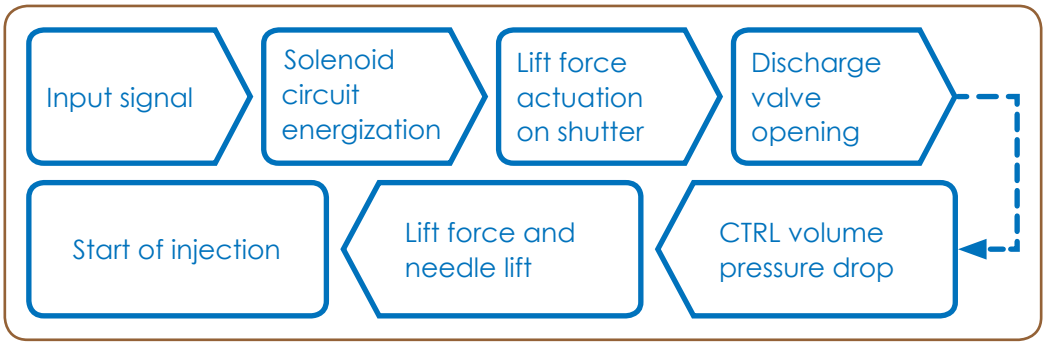

Figure 2 - Intrinsic delay time of each injector component by sequence order

The important note is that a used injector in contrast with a new one, might have a reasonably increased injection delay due to aging. Aging can happen due to deposition and fouling near the injector needle, slowing the hydraulic responses to the electric command. Herein, two fresh injectors have been considered for the experimental study which is described in the next section.

■ Effects of injector's time characteristics on combustion phenomena

Sum of the measured injection time (IT) and the corresponding energizing time is used to determine the start of injection. The Start of Injection (SOI) acts as a controlling parameter of combustion phenomena and engine pollutants. Just to illustrate the importance of SOI, an example of temperature distribution for two cases simulated under the same engine operating condition is shown in Figure 3. As shown, the case with early injection has a higher peak temperature and therefore more chamber walls are exposed to heat release.

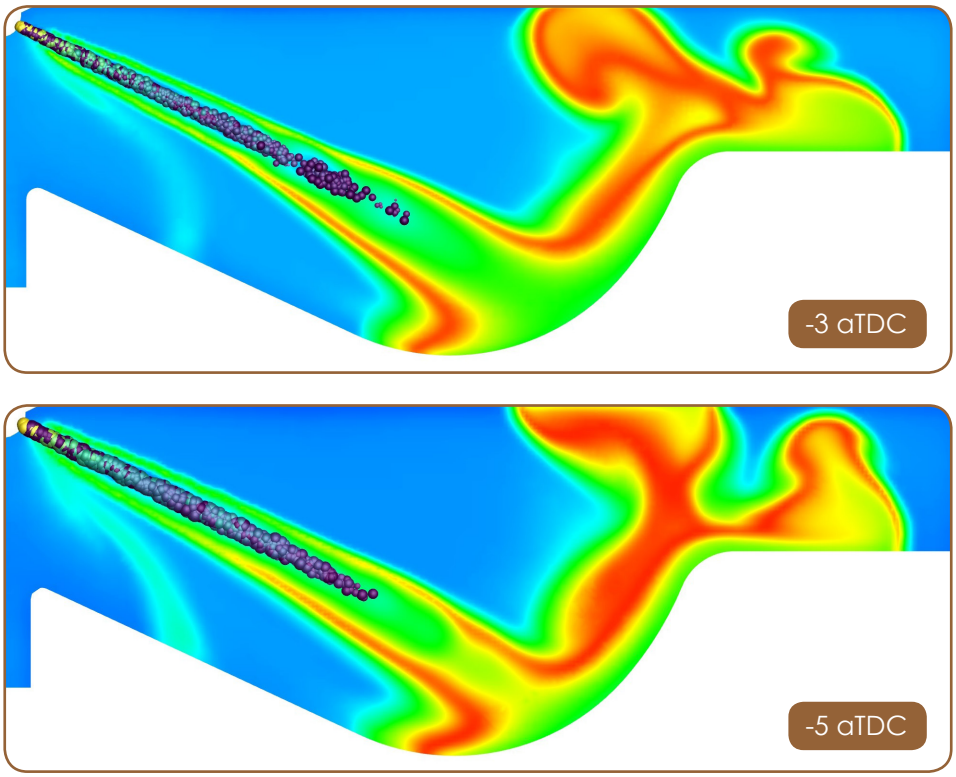

Figure 3 - Temperature distribution for two cases with transition of the start of injection (plotted at +1° CA after top dead center)

Conclusions from our combustion studies on the role of injection time are summarized below:

1. Early injection timing can cause an extended ignition delay owing to the lack of charge-air pressure and temperature required to burn diesel fuel, which in turn increases the homogeneity of air-fuel mixture. This leads to elevated gas temperature and therefore NOx formation while maintaining fuel consumption and smoke at lower levels. Reduction in fuel consumption can be associated with high accumulation of heat release rate around the top dead center, and lower level of smoke with the fuel having more time to burn off. Conversely, late injection timing results in lowered NOx and increased fuel consumption because of increase in the amount of unused enthalpy that will finally exit through the engine exhaust.
2. In general, if start of injection occurs too late (after TDC) or early, ignition delay can be extended in both cases. Therefore, start of injection should be set at an optimal point

such that the right tradeoff between performance and emissions is achieved as a result of the compromise.

3. Furthermore, the injection time impacts the spray-wall impingement; therefore, it should be considered in accordance with the piston-bowl design and liner. Finally, the lifespan of all components of the chamber will be correspondingly affected.

Aforementioned effects are compared and summarized in Table 1. Note that, to have a comparison baseline, a typical variation in injection timing of a diesel engine is applied at the same load and speed; otherwise, the comparison might be biased.

Table 1 - Comparison of ignition timing on engine performance

Item	Early IT	Late IT
Peak pressure	▲	▼
Fuel consumption	▼	▲
Exhaust temperature	▼	▲
NOx level	▲	▼
Smoke level	▼	▲
Spray-wall impingement	Towards Inside of the bowl center	Towards Outside of the bowl center

Experimental Procedure

■ Equipment

The experiment was carried out on a heavy-duty diesel injector with a maximum pressure of 1800 bar and injection volume ranging from 25 to 1000 mm^3 / stroke. The experimental pieces of equipment employed in this study are listed below and the relevant test bench is shown in Figure 4.

- High-speed camera: model PCO 11000 FPS in a frame size of 1280 x 51 pixels
- LED light control board
- LED light stand
- High pressure pump and signal generator
- High pressure pipe, connectors and holders

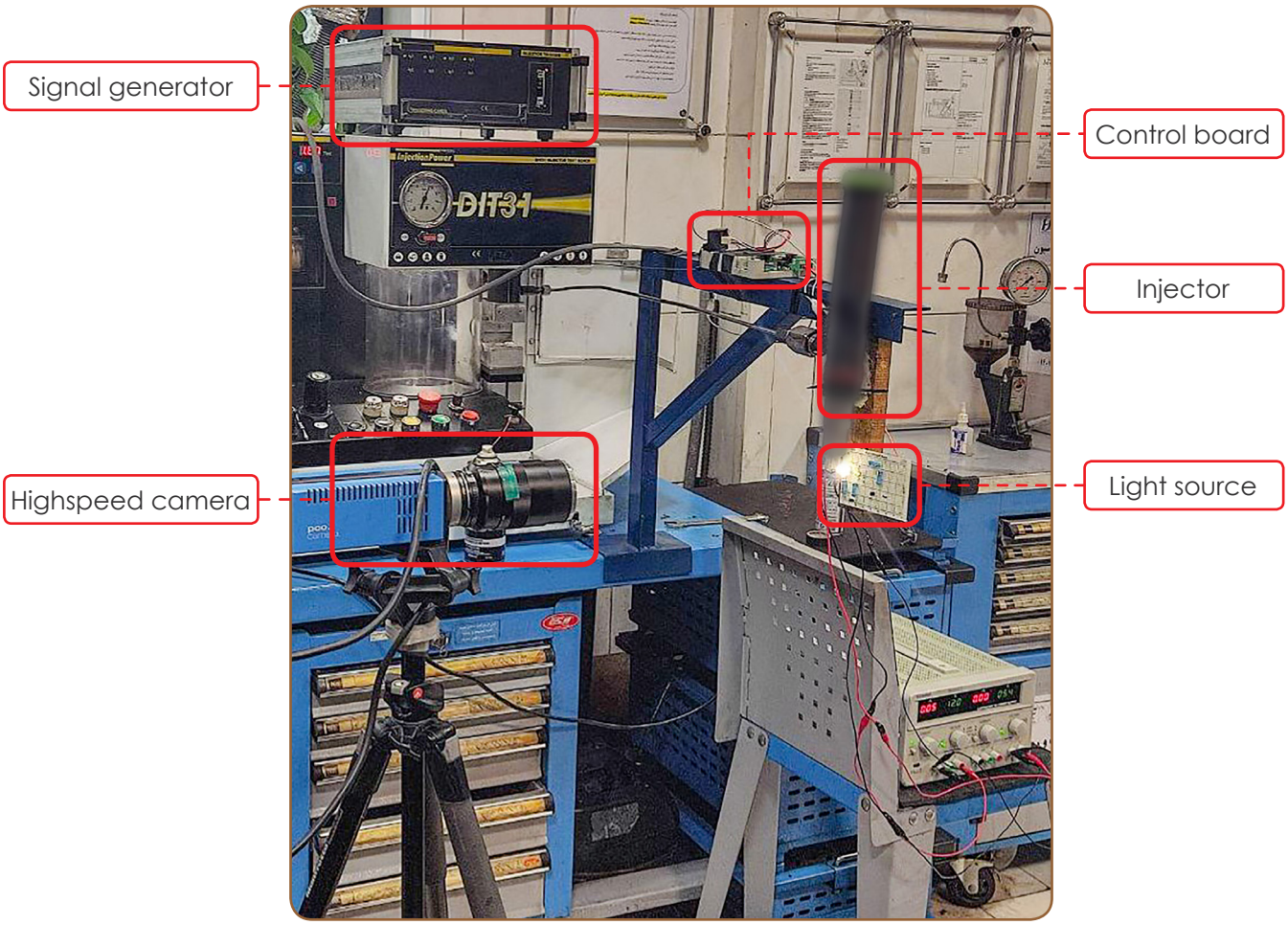

Figure 4 - Test setup for measuring the injection delay time

■ Methodology

In order to recognize the time discrepancy between the applied input signal and the first droplets emerging from the injector holes, an innovative and relatively simple solution was implemented. One primary obstruction to identification of such a time difference is inconsistency in temporal framework of measurement instruments. To overcome this barrier and develop a unique platform for detection of the signal input, start of injection, and end of injection events, a time-aligned connection between them should be prepared. Hence, a means to show ECU signal on the screen had to be established.

In this study, two light sources and a high-speed camera were made use of. The background LED which was permanently emitting light was used to generate the shadows of fuel droplets and help the camera collect the scattered light. The secondary light, defined as the "Signal Light" term, was supplied to monitor the signal activation mode in the scene. Thus, the secondary light source was an LED which was activated directly by the signal entering the injector. Due to negligible delay between the signal and the secondary light emission, LED's ON/OFF condition captured by the high speed camera, would be a relatively precise indicator of the injection signal status. The time difference between successive frames in a sequential locomotion of pictures captured by the high-speed camera with a given number of frames per second (FPS) is of a constant value. Therefore, by counting intermediate frames between captured events we can determine the time interval between them. A brief illustration of the explained concept is depicted in Figure 5.

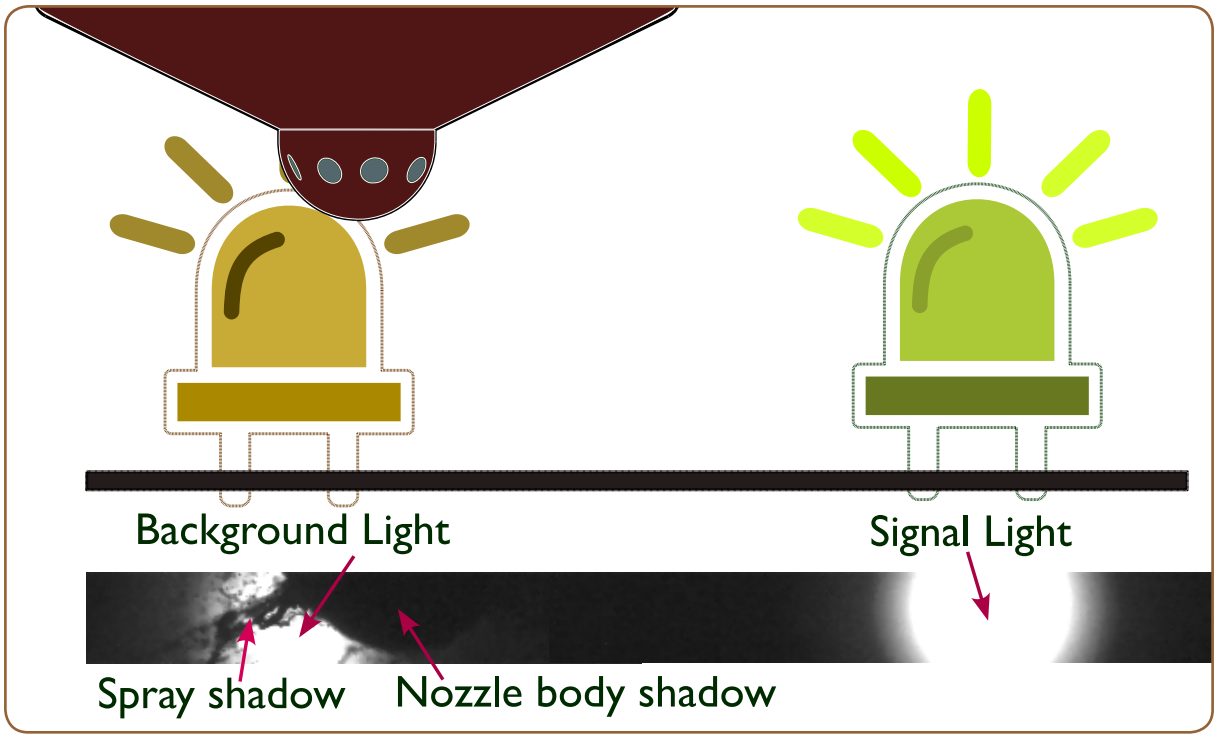

Figure 5 - Schematic of experimental procedure for collecting back light

The following figure shows the experimental procedure done in the lab.

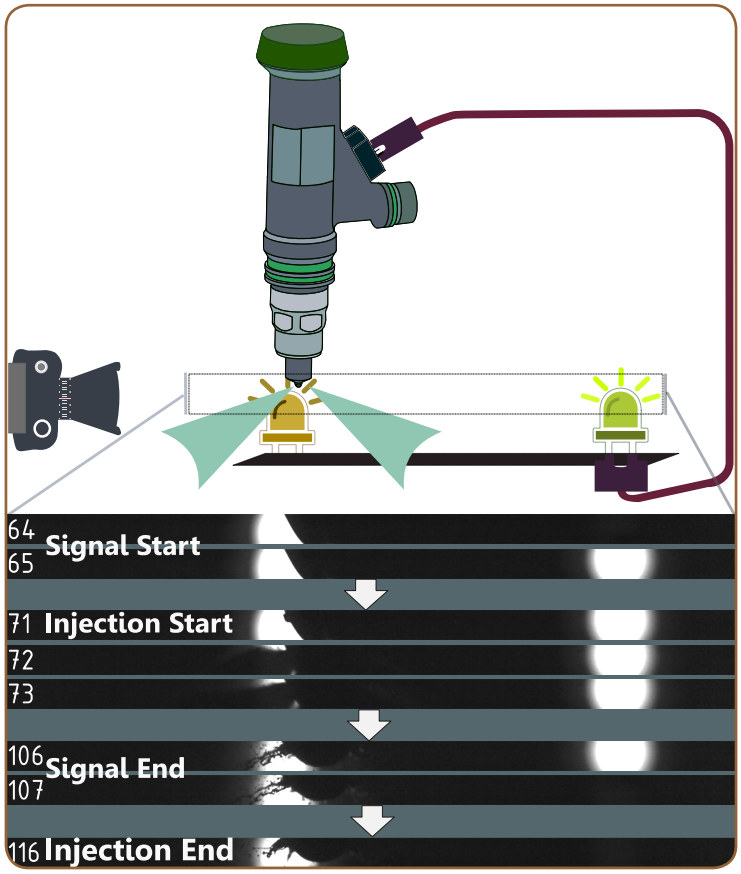

Figure 6 - Schematic of experimental procedure for illustrating back light

To achieve reliable results, two different injectors were used and each injector was studied at 3 different rail pressures of 800, 1400 and 1800 bar with a constant signal duration of 1.837ms. Injection delay and duration for each case are listed in the following table.

Table 2 - Injection delay time for different injection pressure at measured duration times

Injection pressure (bar)	Delay time (µs)		Duration time (µs)	
	Injector #1	Injector #2	Injector #1	Injector #2
800	570	570	2510	2500
1400	540	545	2510	2570
1800	505	530	2570	2570

Concluding Remarks

Sometimes making use of the most common tool for measuring a certain parameter is not the optimum solution; in such a situation making use of the existing infrastructure is beneficial but it would need some degree of innovation to overcome the limitations.

Most injection delay measuring devices, either measure a secondary parameter such as rail pressure which is not a good indicator of the injection start/end detection, or the measured parameter has an inherent asynchronism with the actual event, with an unknown non-constant value. In the present work, the need to measure some instantaneous time parameters regarding diesel injection phenomenon was fulfilled by implementing a new method using high-speed shadowgraphy and a simple optical trick.

This method proved to be a powerful tool to measure the injection delay and injection duration with a measurement tolerance of about 9µs; and capture the actual injection start which makes it a more reliable approach than the conventional methods. The data acquired from this experimental study will be used in the combustion investigations to assess engine performance and components' lifetime studies.

Head Office:
231 Mirdamad Ave. Tehran, I.R.Iran.
P.O.Box: 15875-5643
Tel: +98 (21) 22908581
Fax: +98 (21) 22908654

Factory:
Mapna blvd., Fardis, Karaj, I.R.Iran.
Post code: 31676-43594
Tel: +98 (26) 36630010
Fax: +98 (26) 36612734

www.mapnaturbine.com

GR674-0